Controlling a chaotic array of pulse-coupled circuits

T. L. Carroll
U.S. Naval Research Laboratory, Washington, DC 20375
(Received 10 April 1995)

There has been much attention given to controlling biological systems with pulses, but there has been less attention given to studying the physics of these systems and how the control interacts with the physics. In this work, a set of four circuits intended to simulate the physics of neurons (based on a modified version of the FitzHugh-Nagumo equations) is coupled by pulses, producing a high dimensional system. Numerical simulations and experiments are used to study simple, pulse-based control schemes for this system. A pulse control scheme that requires less knowledge of the system than an Ott-Grebogi-Yorke control scheme is used, and its efficiency is compared to that of periodic pacing and demand pacing.

PACS number(s): 05.45.+b, 87.10.+e

I. INTRODUCTION

There have recently been suggestions that control techniques based on reconstructing return maps from complex time series in biological systems might be useful for controlling abnormal rhythms present in those systems [1,2]. Typically, a series of interlike intervals from a heartbeat or nerve signal is used to construct a first return map. Suspected unstable period one orbits are then located by means of an algorithm that searches for stable and unstable directions in the return map. This information is used to determine when to stimulate the system with a control pulse in order to produce the desired (usually periodic) dynamics.

In most work, these techniques have been used on biological systems for which the dynamics are not known or on low dimensional noisy systems [3,4]. There has been some work on applying control techniques to oscillator networks [5]. There is some controversy over whether or not it is possible to reliably find unstable period one orbits from experimental data in higher dimensional systems using two-dimensional (2D) return maps and on how the control techniques really work, or if they are really new to biology.

In an attempt to understand some of the physics behind these control techniques, this paper reports on studies of a complex circuit model that contains some of the same physics as a group of coupled neurons. Rings of coupled oscillators are believed to be useful for understanding more complex neural networks [6], so a ring configuration of circuits is used. An unstable period 1 orbit is located in the numerical model for the full 12-dimensional flow and from a 2D map-based technique. The map-based technique is also used to find an unstable period 1 orbit in data from the circuit. A simple control technique is then demonstrated on a 2D system and applied to the 12D numerical model and to the circuit. This technique is then compared to existing control techniques for biological systems.

Sepulchre and Babloyantz [5] have used the Ott-Grebogi-Yorke (OGY) control technique [7] in a high dimensional network of coupled oscillators and shown that higher dimensional control is possible. In this paper the OGY technique is not used. The OGY control technique works well when the locations and slopes of the stable and unstable manifolds of an unstable orbit are known, but in experimental data from biological systems it may not always be possible to find this information. It is therefore useful to know how well a control technique that requires less information may perform. A simple pulse technique is studied in this paper, and its efficiency is compared to periodic pacing and demand pacing controls.

II. CIRCUIT MODEL

Actual neurons are quite complicated. For many years, simple approximate models of neurons have been used to understand their basic function [8,9]. It has been shown in many cases that simple models can adequately reproduce some of the basic physics behind the firing of neurons [10–12]. The goal of this work is not to model a specific biological system but to understand the physics behind a control scheme that has been used with different biological systems, so a simple model that reproduces the basic physics should be adequate.

The circuit model used here is based on the FitzHugh-Nagumo equations [8,9], which are often used as a simple model of a neuron. The equations were modified to make coupling them easier and to make them easier to build as circuits. The equations, as used here, are

$$\frac{dx_i}{dt}=\beta[-y_i+g_1(x_i)]\ , \tag{1}$$

$$\frac{dy_i}{dt}=\beta[x_i-3.0g_4(z_i)]\ , \tag{2}$$

$$\frac{dz_i}{dt}=0.0233\beta\left[w(t)-z_i g_2(x_i)+g_3(x_i)+\sum_{j=1}^{4}\alpha_{ij}x_j\right]\ , \tag{3}$$

$$w(t)=\begin{cases} A & \text{if } \dfrac{nT}{\beta}\le t\le\dfrac{(nT+1)}{\beta}\ ,\quad n=1,2,3,\ldots \\ 0.0 & \text{otherwise}\ , \end{cases} \tag{4}$$

$$g_1(x)=\begin{cases}-2.667x+1.2\ , & x\le 0.3\\ 1.333x\ , & 0.3<x\le 4.0\\ -2.667x+15.9\ , & 4.0<x\end{cases} \quad (5)$$

$$g_2(x)=\begin{cases}0.1\ , & x\le 1.4\\ 10.0\ , & x>1.4\end{cases} \quad (6)$$

$$g_3(x)=\begin{cases}0.0\ , & x\le 1.4\\ -15.0\ , & x>1.4\end{cases} \quad (7)$$

$$g_4(z)=\begin{cases}z\ , & z\ge 0\\ 0.0\ , & z<0\end{cases}. \quad (8)$$

No delay term was included, although for delays that are small compared to the memory time constant (0.0233β) the effect on the dynamics should not be large. The time constant β was 10^5 for the circuit but was set equal to 1 for the numerical simulations. These equations are driven by the variable $w(t)$, which is a square pulse with an amplitude A, although a constant voltage may be substituted to make the system self-oscillatory. The driving signal is a simple approximation to driving signals believed to be present in groups of motor neurons [13,14]. The driving period was T. The x signal from oscillator j was multiplied by the coupling constant α_{ij} before being added into oscillator i. In all the examples in this paper, the coupling constants were $\alpha_{ij}=+\alpha$ for $j<i$, $-\alpha$ for $j>i$, and 0 for $j=i$. The oscillators were coupled in a ring, so α_{14} was $+\alpha$ and α_{41} was $-\alpha$.

The function $g_1(x)$ (Fig. 1) was a piecewise linear version of the cubic function in the FitzHugh-Nagumo equations, while $g_2(x)$ discharged the memory when the x variable exceeded a threshold of 1.4 V. A relative refractory period was provided by $g_3(x)$, which initializes the memory with a large negative constant after a firing. The function $g_4(x)$ prevents spurious effects caused when the z variable becomes too negative.

In most cases when the FitzHugh-Nagumo (FHN) equations are used to simulate a single neuron, only two equations are used, with a time factor that differs by a factor of 1000 [15,16]. In this version of the FHN equations, the slow variable is provided by Eq. (3), which acts as a damped integrator that provides some memory of pulses from other circuits. The time scale of Eq. (3) was made as long as practical within the dynamic range limitations of the analog circuit. The driving signal $w(t)$ is an analog of driving signals that are suspected to drive motor neurons [13].

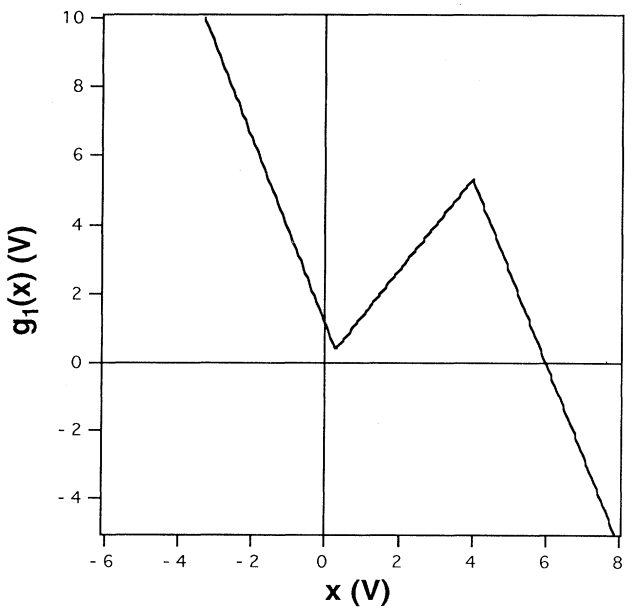

FIG. 1. Graph of function $g_1(x)$ from Eq. (5). This plot was generated numerically.

III. FINDING PERIOD 1 ORBITS

A. Numerical results

To control an unstable periodic orbit, one must know where it is. Equations (1)–(8) were used with a fourth order Runge-Kutta integrator to see if algorithms used to detect unstable period 1 orbits could work with this system [1–4]. The time constant β was set equal to 1.0, while the driving period T was 16.0, the amplitude A was 5.0, and the coupling constant α was 3.0. The x variable for each oscillator was essentially a string of pulses, so the oscillators were pulse-coupled. Figure 2 shows the x variable from each of the four circuits. An interval time series was produced by recording the times at which x_1 exceeded a threshold of 1.4 V. Figure 3 is a first return map plotting the $n+1$th interval I_{n+1} against the nth interval I_n for about 600 data points (the time step used to generate the interval data was 0.04 s). This return map is reminiscent of those seen for interspike interval data from the heart [1]. The largest Lyapunov exponent for Eqs. (1)–(8) with these parameters was calculated [17], and it was found that the system was chaotic, with a largest exponent of 0.014 s^{-1}. This small number may be

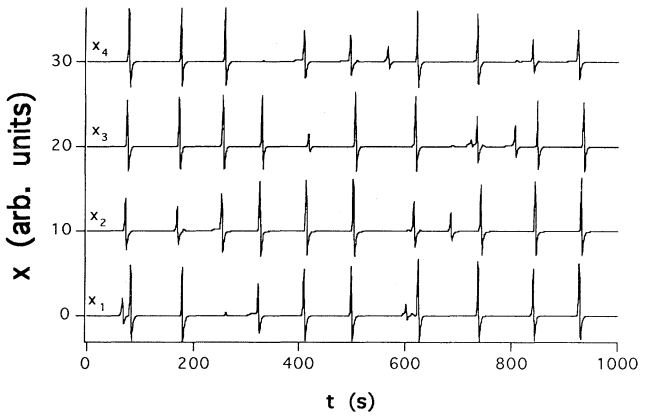

FIG. 2. Time series of the four x variables from numerical simulations of Eqs. (1)–(8). From bottom to top, the signals are x_1, x_2, x_3, and x_4. An offset has been added to the top three signals for clarity.

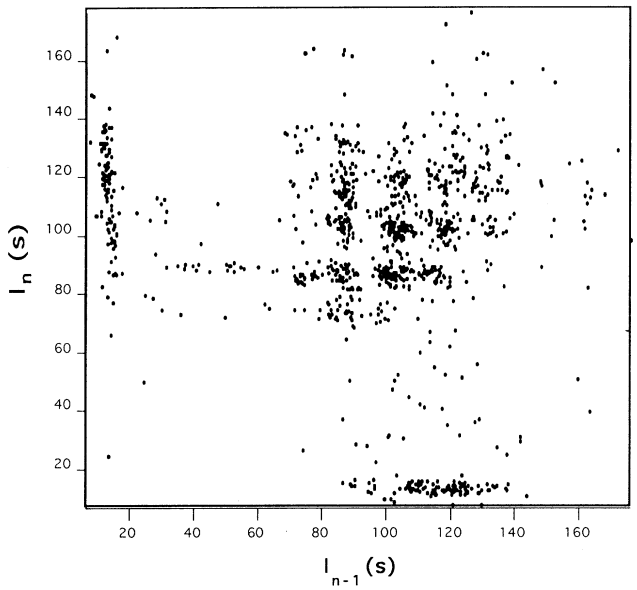

FIG. 3. Return map created by plotting interspike intervals I_n from the x_1 signal from numerical simulations of Eqs. (1)–(8).

slightly misleading, as the coupled oscillators only interact when they fire, while the Lyapunov exponent is averaged over the entire trajectory.

A simple algorithm for detecting unstable period 1 orbits, based on those used in [1–4], was chosen to locate unstable period 1 orbits in these data. This algorithm is defined in the Appendix. The algorithm indicated that there was an unstable period 1 flip saddle with a period of approximately 105 s, a stable eigenvalue of approximately -0.1, and an unstable eigenvalue of approximately -4. The same algorithm was used with a randomly shuffled version of the same time series. The same fixed points were also located in the shuffled data; how to define and use algorithms for finding unstable periodic orbits from interval data is currently being debated [3,4,18], so there may be better algorithms than the one used here.

It was uncertain if the period 1 detection algorithm, which was based on a 2D map, could give accurate results in a system that could be as high as 12 dimensional. A time series of all 12 variables of flow data was generated using the same parameters as above, with a close approach algorithm [19] to find unstable periodic orbits. A time series of 200 000 points with an integrator time step of 0.2 s was used. An unstable period 1 orbit was found with a period of 103 s. The Lyapunov exponents for this orbit were calculated from Eqs. (1)–(8), using the method of Eckmann and Ruelle [17]. The largest exponent was 0.005 s^{-1}, while all others were negative. The fact that this orbit had only one unstable direction makes it highly likely that it could be stabilized by a single control signal [5,7]. The magnitude of this exponent was not compared directly to the unstable eigenvalue determined from the interval map because there is no simple way to transform from the time series representation to the interval map.

As a check on the detection algorithm, a second set of time series was generated for a self-oscillatory configuration. In this case, the driving signal $w(t)$ was set equal to a constant of 1.2. The sample coupling configuration was used with a coupling constant α of 8.0. The resulting 2D return map was very complex, with no obvious structure (it resembled return maps generated from electrical signals from the brain [2]). The period 1 detection algorithm based on the interval return map indicated a period 1 flip saddle with a period of 29 s, but the method of close approaches used with the full flow did not find any fixed points. It is possible that the period 1 orbit was too unstable to be detected with the close approach method, as this configuration was found to have two positive Lyapunov exponents. There are other methods for finding periodic orbits numerically [20], but they require a good estimate for the location of the orbit and would be very cumbersome of this system.

B. Experimental results

The same map-based period 1 detection algorithm was used with data from four actual FHN circuits, coupled in the manner described above. The time constant β for the circuit was 10^5 s^{-1}, while the driving period T was 1.144 ms, the amplitude A was 14.0, and the coupling constant α was 8.0. Figure 4 shows time series of the x variables of all four circuits; from bottom to top, the signals are x_1, x_2, x_3, and x_4. Figure 5 is the interval return map from the circuit.

A false nearest neighbor algorithm [21] was used to find the embedding dimension of a time series of 100 000 intervals from the circuit. In this type of algorithm, a data point is defined as a near neighbor in phase space if it is within some distance ε of a reference point. When the embedding dimension is increased, the distance between the data point and the reference point will increase because of the added dimension, but it may increase more than can be accounted for by the dimension increase.

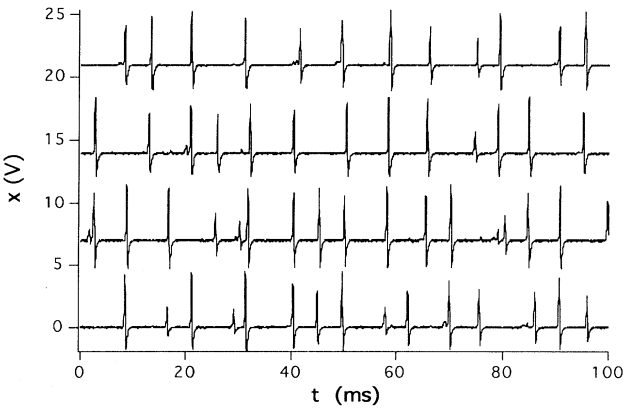

FIG. 4. Time series of the four x signals from a coupled circuit array based on Eqs. (1)–(8). From bottom to top, the signals are x_1, x_2, x_3, and x_4. An offset has been added to the top three signals for clarity.

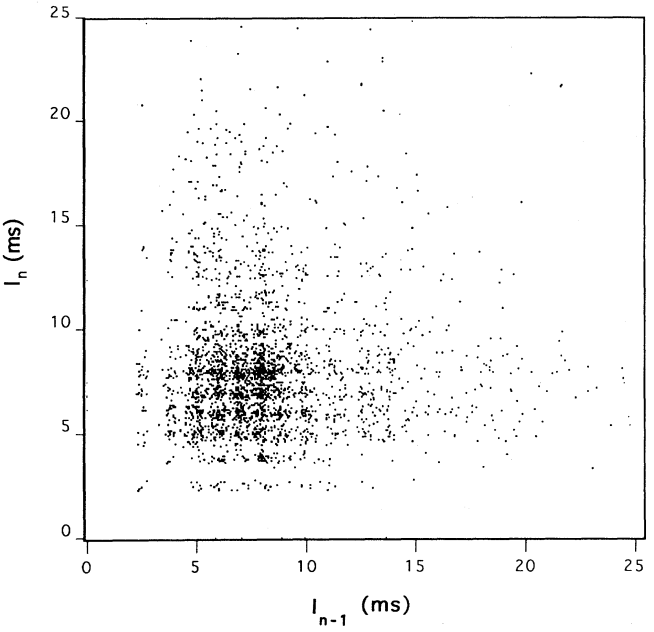

FIG. 5. Return map created by plotting interspike intervals I_n from the x_j signal from a coupled circuit array based on Eqs. (1)–(8).

Such a data point is a false nearest neighbor. When the data embedding dimension is increased to the point where it exceeds the attractor embedding dimension, the fraction of data points that are false nearest neighbors should fall off sharply. Such a fall off was not seen for the time series of 100 000 intervals from the circuit for data embedding dimensions as high as 14, so it could not be distinguished from noise. The false nearest neighbor technique should work with higher dimensional data, and it should be possible to analyze interval data in this way [22]. It may be that the intervals were long enough, compared to the largest Lyapunov exponent for the system, that using interval data undersamples the dynamics. Because no reliable embedding dimension estimate was available, no Lyapunov exponent calculation was attempted.

The 2D map-based algorithm for period 1 detection found possible period 1 flip saddles with periods of about 7.8, 5.9, and 6.8 ms. The method of close returns was not used to find fixed points because a 12 channel digitizer with sufficient speed was not available.

IV. CONTROL

A. Numerical results

Once the unstable period 1 orbits have been detected, it may be possible to stabilize them. In [1], once an unstable fixed point is found from the interval return map, the stable and unstable manifolds of this point are also found. One may then predict that if the system approaches the fixed point along its stable manifold, it will then move away from the fixed point along its unstable manifold. This predictability allows intervention in the system through a control pulse that forces the system back onto the stable manifold of the fixed point when it starts to move away. In [1], the application of this algorithm actually produced a period 3 orbit, not the desired period 1. This algorithm was also applied in [2], but there are suggestions that in some cases this type of pulsed control amounted to what is known as demand pacing, where the system is forced to fire if it goes longer than some fixed time without firing [4,23].

Sepulchre and Babloyantz [5] demonstrated OGY control in a high dimensional oscillator network, but their work was numerical, so they had all of the necessary information to implement the OGY algorithm. It is possible that the 2D map method for finding fixed points and manifolds could be extended to higher dimensions, but it is likely that the amount of data required to give dependable results would rise quickly. In biological systems, there is usually not time to take a long time series. As a result, the aim here is to first try a very crude control technique that does not need too much information.

To find a control method for the circuit array used here, it was necessary to test the predictability of the interval data. Stable and unstable manifolds for the unstable fixed points were estimated from interval return maps generated by Eqs. (1)–(8) (Fig. 3) or the corresponding circuit (Fig. 5). Attempts were made to use these calculated manifolds to predict the motion of the system near the fixed point; when the system approached the fixed point along the stable manifold, the unstable manifold was used to predict the next interval. It was possible in most cases to predict that a point on one side of the line of identity would be followed by a point on the other side, but it was not possible to predict how far from the line this point would be, so it is likely that the calculated manifolds were not good approximations to the real manifolds. While the numerically generated unstable period 1 orbit from Eqs. (1)–(8) did have only one unstable direction, this direction occupied a space of as many as 12 dimensions. The interval map calculation gives the projection of this manifold into two dimensions, so much information is lost.

A very simple control algorithm was designed that relied on the fact that if the point on the interval map I_{n-1}, I_n was on one side of the line of identity, the point I_n, I_{n+1} would usually be on the other side. If the interval I_{n-1} between successive firings was less than the fixed point I_f but greater than some minimum value $I_{\min}$, a small pulse was added to the driving signal $w(t)$ after oscillator 1 finished firing. This pulse by itself was not enough to cause any of the oscillators to fire, but since the oscillators did retain some memory of the driving inputs, it could cause the next interval I_n to be shorter than it would have been. The amplitude of this pulse was proportional to the difference $I_f - I_{n-1}$. For convenience, this control will be called subthreshold pulse feedback (STPF) control.

The way that this STPF control algorithm works may be shown for numerical simulation of a single uncoupled FHN oscillator with a drive period T of 16 s and a driv-

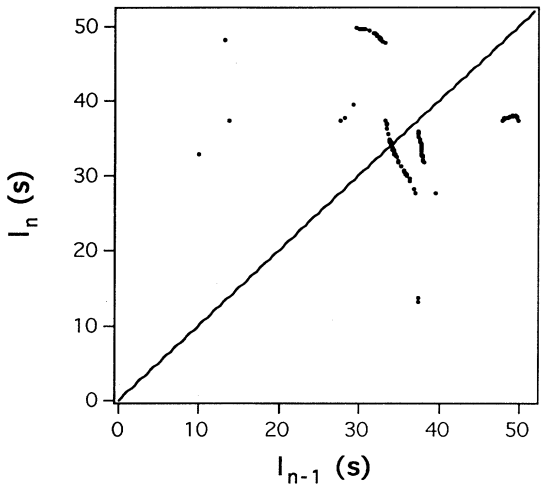

FIG. 6. Interval return map created from interspike intervals I_n from the x variable from a numerical simulation of a single driven uncoupled FitzHugh-Nagumo system.

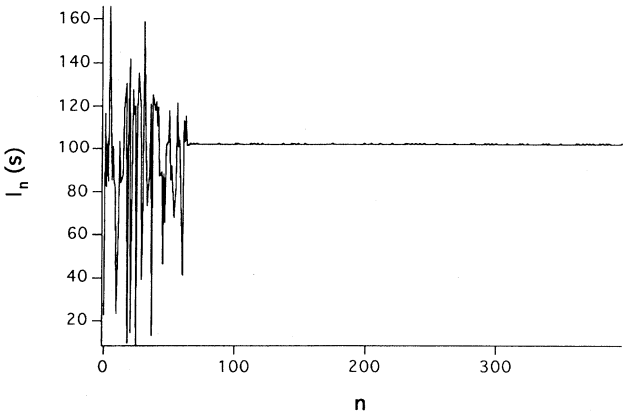

FIG. 8. Time series showing interspike intervals I_n for a numerical simulation of Eqs. (1)–(8) when a STPF control algorithm has been activated. The control algorithm was activated at $n=0$, causing a short transient followed by a controlled period 1 orbit with a period of 102 s.

ing amplitude A of 14.0. An interval return map for this system is shown in Fig. 6. The output from this system looks like a one-dimensional map and crosses the line of identity with a slope of -3.0 at a fixed point value of $I_f=34.02$ s. Adding a control pulse to shorten the next firing interval should change the slope of this map. Adding a pulse with a fixed height of 0.1 when the system is near the fixed point shortened the next interval by 0.25 s. For control, the height of the added pulse was $\gamma(I_f-I_{n-1})$ when I_{n-1} was between 33.6 and 34.02 s. To make the slope of the unstable manifold less negative than -1.0, γ must be at least 0.8. Figure 7 shows an enlargement of the map in Fig. 6 when the control has been activated with $\gamma=0.7$; a portion of the unstable manifold has been tilted so that its slope is only slightly more negative than -1.0. For $\gamma=0.8$, the slope of this portion of the manifold becomes less negative than -1, and after a very short transient the system reaches a stable period 1 orbit. This control technique is similar to the map-based technique of Petrov, Peng, and Showalter [24].

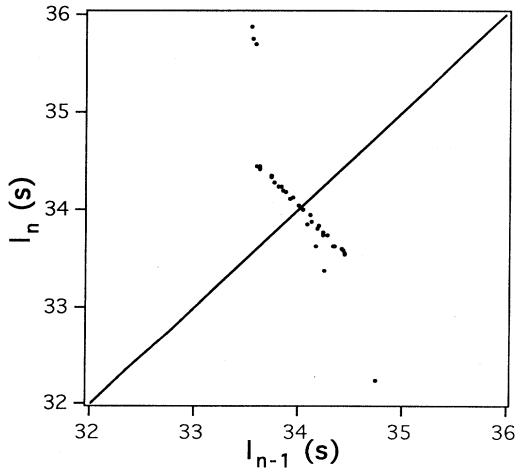

FIG. 7. Blowup of the map of Fig. 5 when STPF control has been activated with a feedback constant γ of 0.7, just under that needed to control the system.

This same STPF control technique was also applied to the full coupled system of Eqs. (1)–(8) by adding the control pulse to the driving signal $w(t)$ for all four oscillators. Because the return map was more than two-dimensional, it was not possible to calibrate the effect of a fixed pulse on the interval timing; thus a constant γ was chosen by trial and error. When a control window between 100 and 107 s was used with $\gamma=0.25$, the system stabilized to fixed point of 102.3 s (Fig. 3), near the actual fixed point of 102.3 s. The fact that the upper end of the control window is above the fixed point is still consistent with this type of control; all that is required is that the unstable manifold be rotated to cross the identity line with a slope less negative than -1.0. If the upper end of the control window is above the fixed point, the controlled point will be below the fixed point.

To judge if the STPF control algorithm might be able to create period 1 orbits far from the fixed point, the same control technique was used for windows extending between 85 and 90 s or 180 to 185 s. No control was seen in either of these cases.

The control did not work when the control pulse was applied to only a single oscillator; it is probable that there are various spatial modes that exist for this coupled system, and controlling these modes may require control at more than one point. Control of spatially extended systems is a topic of ongoing research [25].

B. Experimental control

An analog controller circuit was built to see if this STPF control method would work in a high dimensional circuit. The control circuit charged a capacitor to keep track of the time since the last firing of one of the oscilla-

tors. When the x signal from oscillator 1 exceeded 1.4 V, the voltage V_s on the capacitor was sampled by a sample and hold amplifier, after which the capacitor voltage was reset to 0. When this sampled voltage V_s was within a 2.0 V window below the control voltage V_c, the control circuit produced a pulse S_c with an amplitude of $\gamma(V_c - V_s)$ (where γ was 8.3) and a width of 0.1 ms. This pulse by itself was much smaller than the drive pulses $w(t)$; a typical comparison of the power delivered by drive and control pulses is given below. The control voltage V_c was varied until a controlled period 1 orbit was seen. When the driving period T was 1.144 ms, the amplitude A was 14.0 V, and the coupling constant α was 8.0, it was possible to control a fixed point at 6.88 ms.

Figure 9 shows the controlled period 1 orbit, which follows a transient as the controller was turned on. This controlled orbit appears to correspond to one of the orbits detected by a period 1 detection algorithm, but as discussed in the caption it may be a new orbit created by the control. Figure 10 shows the x signal from each of the four FHN circuits, the control signal S_c, and the driving pulses when the circuits are in the controlled period 1 orbit. For comparison to other control methods, the average power delivered to the FHN circuit array by the control circuit was calculated to be 5.6 mW, while the drive signal here delivered 41 mW. Some of the power delivered by the control signal was lost because the control pulse began while the circuits were still discharging [$g_2(x)$ in Eq. (6) was still 10.0], so the circuits were not sensitive to the entire control pulse. This could be corrected by increasing the delay between the circuit firing and the control pulse.

Because the control algorithm here changes the unstable manifold by rotating it downward, it is possible for the manifold to cross the line of identity below the original fixed point, creating a new fixed point. This effect was probably seen when the four circuits were driven with a period T of 3.185 ms, an amplitude A of 14.0, and a coupling constant α of 3.0. In this case, the map-based period 1 finding algorithm gives a fixed point of 12.7 ms, while the pulse control technique results in a stable period 1 orbit of about 9.5 ms.

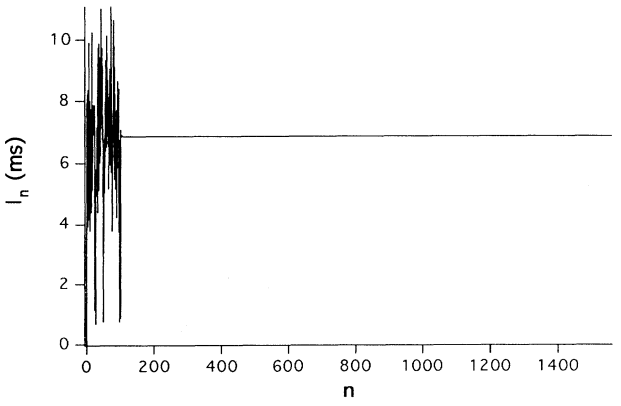

FIG. 9. Time series showing interspike intervals I_n for the x_1 signal from an array of coupled circuits based on Eqs. (1)–(8) when an analog STPF controller has been activated. The controller was activated at $n=0$, causing a short transient followed by a controlled period 1 orbit with a period of 6.88 ms.

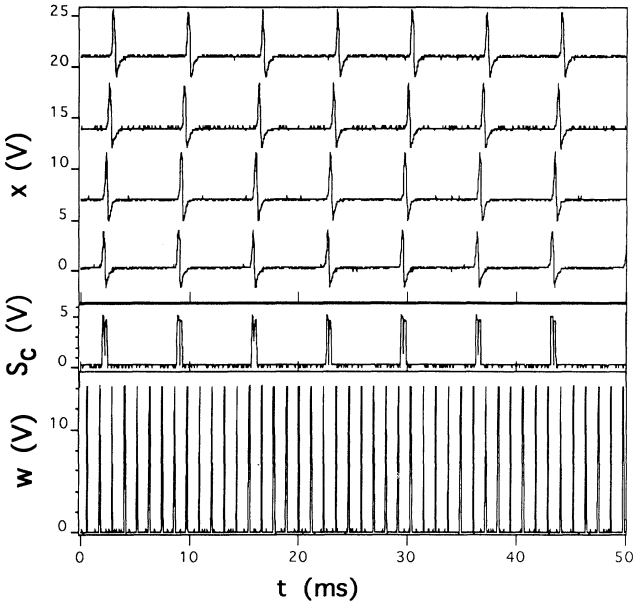

FIG. 10. Time series from a controlled array of coupled circuits based on Eqs. (1)–(8) when a STPF controller has been activated. The lowest trace shows the driving signal $w(t)$; the next trace up shows the STPF control signal S_c; and the top four traces show x_1, x_2, x_3, and x_4, in that order. The top three signals have been offset for clarity. The control signal is nonzero because the system is not on the fixed point for the unperturbed system. It is possible to bend the unstable manifold so that it crosses the line of identity below the original fixed point, creating a new stable fixed point (this has been seen in the single-oscillator simulations). The controlled fixed point is at 6.88 ms, which is below one of the detected unstable fixed points at 7.8 ms.

C. Comparison to other control techniques

It is useful to compare this control technique to other control techniques that might be used in a biological system in order to determine if it is better, worse, or the same as the other methods and to show that it is indeed different. The STPF control method described above was compared to periodic pacing, in which a periodic pulse train is used to entrain the system, and demand pacing [23], where the system is forced to fire if some maximum interval passes without it firing. For these experiments, the driving period T for the circuit was set to 1.144 ms, the driving amplitude A was set to 14.0 V, and the coupling constant α was 8.0.

1. Periodic pacing

For the periodic pacing, a large entraining pulse was necessary. Entrainment was seen for an entraining pulse

period of 5.0 ms, a height of 14.0 V, and a width of 400 μs, or four times the size of the driving pulses. The average power delivered by the controlling circuit to the FHN circuits during entrainment was about 26 mW. It was possible to entrain the FHN circuit array to other pulse periods, but this required even larger entrainment pulses.

2. *Demand pacing*

It was possible to drive the circuit array into many different period 1 and period 2 orbits using demand pacing, but most of these did not correspond to suspected periodic orbits of the system and were not predictable without knowing the system dynamics. To produce a period 1 orbit with a period of 5.76 ms, the controller delivered an average power of 5.8 mW. There were many such orbits seen as the control voltage was changed. Glass and Zeng [23] discuss targeting particular orbits for demand pacing.

Because the controller prevented any pulses longer than a certain maximum, it was always possible to get a series of intervals such as the one in Fig. 11, where the maximum interval was 5.04 ms. This type of control required a larger controller signal, however; the power delivered by the control circuit was 21 mW.

V. CONCLUSIONS

Previous attempts to control systems with pulses have used poorly characterized or very simple systems. This work presents an intermediate case, a system that is complex but well defined. It was shown that simple control techniques can work on higher dimensional deterministic systems, and the efficiency of different control techniques was compared. The most efficient control was one that used control pulses that were not large enough to make the system fire immediately, here called a STPF technique. This method worked by modifying the dynamics of the system near an unstable fixed point, as is suggested in [1]. The least efficient method was periodic pacing, although periodic pacing will always work for a large enough entrainment pulse. Demand pacing for this circuit could be as efficient as STPF control when it interacted with the system dynamics to produce a period 1 orbit, but it required more power to generate a time series with an arbitrary maximum period. The main disadvantage of the STPF technique was that it required more information about the system and was not as robust as the other two techniques.

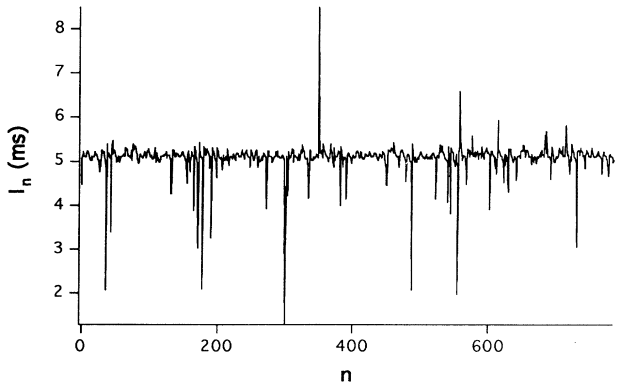

FIG. 11. Time series of intervals I_n when demand control is used with the coupled circuit array.

The STPF technique could probably be improved by using more information about the system. It has been suggested that it might be better to use more than one signal from a biological system in order to find fixed points [2]. It makes sense that a 2D return map is not the best way to find fixed points and manifolds in a possible higher dimensional system. The control response could also be made higher dimensional by applying different pulses to different parts of the system [5]. While there are good control techniques for higher dimensional systems, there are still problems applying them to biological systems, where the amount of knowledge about the system is limited.

APPENDIX: PERIOD 1 DETECTION ALGORITHM

The algorithm for detecting fixed points in this work was different from the algorithm of Pierson and Moss [3]. In many cases, the system state is seen to linger near the unstable period one orbit for several cycles. The algorithm described here allows for this possibility.

A one-dimensional time series of intervals I_n between firings of the x variable of oscillator 1 is stored and used to construct a first return map of (I_{n-1},I_n). These points are labeled (x_n,y_n). First, the data are searched for a point where the absolute value of x_n-y_n is less than 10% of the data range. These points may appear in groups, so the following points are checked to see if this condition holds. There will be a total J of these points. The fixed point location is taken as the average of these points. Next, the numbers Δ_i are calculated, where $\Delta_1=\text{abs}(x_{n-2}-y_{n-2})$, $\Delta_2=\text{abs}(x_{n-1}-y_{n-1})$, $\Delta_3=\text{abs}(x_{n+J+1}-y_{n+J+1})$, and $\Delta_4=\text{abs}(x_{n+J+2}-y_{n+J+2})$. For the points before the fixed point to be moving away from the line of identity and the points after the fixed point to be moving away, $\Delta_1>\Delta_2$ and $\Delta_3<\Delta_4$. The points must be moving away at an increasing rate, so it is required that $\Delta_1>C\Delta_2$ and $C\Delta_3<\Delta_4$, where C is a constant greater than 1. C is arbitrarily set equal to 2.0. For groups of points that satisfy these conditions, the slopes of the incoming and outgoing manifolds must be calculated. The slope m_s of the stable manifold is taken as the average of the slopes of the lines connecting the points (x_{n-2},y_{n-2}) to (x_{n-1},y_{n-1}) and (x_{n-1},y_{n-1}) to (x_n,y_n). The slope m_u of the unstable manifold is taken in an analogous fashion. The final requirement is that $0<m_s<-1.0$ and $-1.0<m_u$. The negative signs on the slopes also force the candidate fixed point to be a flip saddle. To qualify as a fixed point, multiple candidates must be found within 10% of each other and have values for the unstable manifold slope m_{us} within 20% of each other. The stable manifold slopes were small enough that a small difference in point locations could produce a large difference in slope, so the stable manifold slopes were not used to differentiate fixed points.

[1] A. Garfinkel, M. L. Spano, W. L. Ditto, and J. N. Weiss, Science **257**, 1230 (1992).
[2] S. J. Schiff, K. Jerger, D. H. Duong, T. Chang, M. L. Spano, and W. L. Ditto, Nature (London) **370**, 615 (1994).
[3] D. Pierson and F. Moss, Phys. Rev. Lett. **75**, 2124 (1995).
[4] D. J. Christini and J. J. Collins, Phys. Rev. E (to be published).
[5] J. A. Sepulchre and A. Babloyantz, Phys. Rev. E **48**, 945 (1993).
[6] J. J. Collins and I. Stewart, Biol. Cyber. **71**, 95 (1994).
[7] F. J. Romeiras, C. Grebogi, E. Ott, and W. P. Dayawansa, Physica D **58**, 165 (1992).
[8] R. FitzHugh, Biophys. J. **1**, 445 (1961).
[9] J. Nagumo, S. Arimoto, and S. Yoshizawa, Proc. IRE **50**, 2061 (1962).
[10] R. E. Mirollo and S. H. Strogatz, SIAM J. Appl. Math. **50**, 1645 (1990).
[11] K. Wiesenfeld, Phys. Rev. Lett. **72**, 2125 (1994).
[12] See, for example, Proceedings of the NATO ARW Stochastic Resonance in Physics and Biology, edited by F. Moss, A. Bulsara, and M. F. Schesinger [J. Stat. Phys. **70**, 1 (1993)].
[13] J. J. Collins and S. A. Richmond, Biol. Cyber. **71**, 375 (1994).
[14] C. J. DeLuca, A. M. Roy, and Z. Erim, J. Neurophys. **70**, 2010 (1993).
[15] F. Moss, J. K. Douglass, L. Wilkens, D. Pierson, and E. Pantazelou, in *Stochastic Processes in Astrophysics* (New York Academy of Sciences, New York, 1993).
[16] D. Petracchi, M. Barbi, S. Chillemi, E. Pantazelou, D. Pierson, C. Dames, L. Wilkens, and F. Moss, Int. J. Bifurc. Chaos **5**, 89 (1995).
[17] J.-P. Eckmann and D. Ruelle, Rev. Mod. Phys. **57**, 617 (1985).
[18] L. M. Pecora (unpublished).
[19] D. Auerbach, P. Cvitanovic, J.-P. Eckmann, G. Gunaratne, and I. Procaccia, Phys. Rev. Lett. **58**, 2387 (1987).
[20] T. S. Parker and L. O. Chua, *Practical Numerical Algorithms for Chaotic Systems* (Springer-Verlag, New York, 1989).
[21] M. B. Kennel, R. Brown, and H. D. I. A. Abarbanel, Phys. Rev. A **45**, 3403 (1992).
[22] T. Sauer, Phys. Rev. Lett. **72**, 3811 (1994).
[23] L. Glass and W. Zeng, Int. J. Bifurc. Chaos **4**, 1061 (1994).
[24] V. Petrov, B. Peng, and K. Showalter, J. Chem. Phys. **96**, 7506 (1992).
[25] Y.-C. Lai and C. Grebogi, Phys. Rev. E **50**, 1894 (1994).